

# Analysis of improvements in MOPITT observational coverage over Canada

Heba S. Marey<sup>1</sup>, James R. Drummond<sup>1</sup>, Dylan B. A. Jones<sup>1</sup>, Helen Worden<sup>2</sup>, Merritt N. Deeter<sup>2</sup>,  
John Gille<sup>2</sup>, and Debbie Mao<sup>2</sup>

<sup>1</sup> University of Toronto, Department of Physics, Atmospheric Science Group, Ontario, Canada, <sup>2</sup> National Center for Atmospheric Research,  
Boulder, Colorado, USA.

## Abstract

The Measurements of Pollution in the Troposphere (MOPITT) satellite instrument has been measuring global tropospheric carbon monoxide (CO) since March 2000, providing the longest nearly continuous record of CO from space. During its long mission, the data processing algorithms have been updated to improve the quality of CO retrievals and the sensitivity to the lower troposphere. Currently, MOPITT retrievals are only performed for clear-sky observations or over low clouds for ocean scenes. The cloud detection scheme was modified in the new V9 product, resulting in an improvement in observational coverage, especially over land. Comparison of the spatial and seasonal variations of the data coverage in V9 and V8 shows differences with significant geographical and temporal variability, with some regions such as Canada and the Amazon exhibiting a doubling of data in winter. Here we conducted an analysis of Moderate Resolution Imaging Spectroradiometer (MODIS) cloud heights and cloud mask products along with MOPITT retrieval cloud flag descriptors to understand the impact of cloud conditions on the MOPITT observational coverage, with a particular focus on observations over Canada. The MOPITT CO total column (TC) data were modified by turning off the cloud detection scheme to allow a CO retrieval result regardless of their cloud status. Analyses of the standard V8 CO TC product (cloud filtered) and non-standard product (non-cloud masked) were conducted for selected days. Results showed some coherent structures that were observed frequently in the non-masked CO product that was not present in the V8 product and could potentially be actual CO features. Many times, these CO plumes were also seen in the Infrared Atmospheric Sounding Interferometer

32 (IASI) CO TC product. The MODIS cloud height analysis revealed that a significant number of  
33 low cloud CO retrievals were discarded in the V8 product. Most of the missed CO plumes in the  
34 V8 product are now detected in the new V9 product as a result of the dependence of MOPITT  
35 radiance ratio (MRT) test over land. Comparisons of the MRT and MODIS cloud height data in-  
36 dicate a remarkable negative correlation. As a result of modified V9 cloud detection algorithm, a  
37 significant portion of the low cloud CO retrievals is now incorporated in the new V9 MOPITT  
38 product. Consequently, the observational coverage over Canada is significantly improved, which  
39 benefits analyses of regional CO variability, especially during extreme pollution events. We also  
40 conducted a comparison of MOPITT and IASI CO TC and found generally good agreement, with  
41 about a 5-10% positive bias that increases in highly polluted scenes.

42

43

#### 44 **1. Introduction**

45 Carbon monoxide (CO) in the atmosphere has a medium lifetime (weeks to months), which is  
46 long enough to track atmospheric physical and chemical processes over a range of spatial scales  
47 from space (Jiang et al., 2011, Edwards et al., 2006; Duncan et al., 2007). Hence, satellite meas-  
48 urements of atmospheric CO are useful for studying both transported and local sources of pollution  
49 as well as atmospheric chemistry.

50 The Measurements of Pollution in the Troposphere (MOPITT) satellite instrument provides  
51 the longest dataset of CO from space. It has been measuring tropospheric CO using gas filter cor-  
52 relation radiometry (GFCR) since March 2000 (Drummond et al., 1996, Drummond et al., 2010,  
53 Deeter et al., 2017), with a footprint of  $22 \text{ km} \times 22 \text{ km}$  and global coverage every 3 days (Deeter  
54 et al., 2003). It is on board the Terra satellite, which is in a sun-synchronous polar orbit at 705 km  
55 of altitude and crosses the equator at 10:30 local time (Drummond et al., 1996). Furthermore, it is  
56 the only satellite instrument that measures CO in both the thermal infrared (TIR,  $4.7 \mu\text{m}$ ) and near  
57 infrared (NIR,  $2.3 \mu\text{m}$ ). This long-term data record provides a unique opportunity for analyzing  
58 interannual variability and long-term trends in the distribution of CO, atmospheric transport, and  
59 tropospheric chemistry that are associated with human activity and climate change (Worden et al.,  
60 2013; Strode et al., 2013, Buchholz et al., 2021).

61 During MOPITT's long mission, data processing algorithms have been updated considerably  
62 to improve the quality of the CO retrievals and their sensitivity to the lower troposphere. However,



63 MOPITT cannot “see” through cloud and this represents a significant obstruction to measurement  
64 spatial coverage. The current cloud detection algorithm, using both MOPITT and Moderate Reso-  
65 lution Imaging Spectroradiometer (MODIS) information (Warner, et al., 2001), rejects pixels with  
66 a significantly amount of cloud cover, thereby reducing the number of pixels retrieved. This leads  
67 to global maps with gaps in CO data where clouds are present.

68 Retrieving CO gas in cloudy conditions represents a major challenge. The presence of clouds  
69 in the observed scene enhances reflectivity and blocks the atmosphere below the clouds for cloudy  
70 scenes compared to cloud-free sky scenes. The albedo and in-cloud absorption effects enhance the  
71 sensitivity to trace gases above the clouds, while the shielding effect impacts the vertical sensitivity  
72 of the measurement which results in an inaccurate estimation of the trace gas column. Various  
73 techniques have been proposed to cope with this problem depending on the spectral range of the  
74 measurements. These techniques can be grouped into the following four approaches.

75 The first approach is the threshold method, where only observations under clear sky conditions  
76 or weakly cloud contaminated scenes (determined by using threshold-based algorithms to detect  
77 clouds and develop cloud masks) are considered (Ackerman et al., 1998; Deeter, 2003; Warner, et  
78 al., 2001). The second approach, referred to as cloud clearing, is to reconstruct clear column radi-  
79 ances that would have been present if there were no clouds. Cloud clearing is used for Atmospheric  
80 Infrared Sounder (AIRS) atmospheric CO retrievals where a reconstructed pixel consisting of a 3  
81 x 3 array (9 pixels are used) is produced, resulting in 45 km spatial resolution (Susskind et al.,  
82 2003; Li et al., 2005). Both of these approaches avoid the need for complex modeling of cloud  
83 effects, but have the added complexity of characterizing errors resulting from un-modeled cloud  
84 fields. The third approach is to solve for the radiative effects of clouds directly in the inversion  
85 process. This approach is used for retrieving profiles (Kulawik et al. 2006) from measurements  
86 from the Tropospheric Emission Spectrometer (TES). The fourth approach is utilized for CO re-  
87 trievals over land and ocean in the presence of low-altitude clouds from measurements from the  
88 TROPOspheric Monitoring Instrument (TROPOMI). In this approach, shortwave infrared (SWIR)  
89 measurements of methane TC are used to filter out observations with high and optically thick  
90 clouds to retrieve the trace gas information (Vidot et al. 2012, Landgraf et al., 2016).

91 For MOPITT, due to the lack of spectral information and collocated methane data, only the  
92 first two approaches are possible and, unfortunately, the results of the reconstructed clear column  
93 radiances using two adjacent pixels are not sufficiently precise for viable retrievals. Consequently,

94 adjustments to the current MOPITT cloud detection scheme is the only one of the four approaches  
95 that can be employed.

96 Deeter et al., (2021) recently made significant changes to the cloud detection scheme resulting  
97 in a new MOPITT product V9. Those changes impacted the MOPITT coverage rate, especially  
98 over land. Hence, the aim of this study is to conduct an analysis of MODIS cloud heights and cloud  
99 mask products along with MOPITT retrieval cloud flag descriptors to understand the impact of  
100 cloud conditions on the MOPITT observational coverage, with a particular focus on observations  
101 over Canada.

102

## 103 **2. Data and Methodology**

104 This study uses data from three satellite instruments, MOPITT, IASI, and MODIS. MODIS,  
105 and MOPITT are all onboard the Terra satellite (with an equatorial crossing time of 10:30 am local  
106 time (LT)), which facilitates the collocation of observations in space and time. IASI on MetOp-A  
107 has an equatorial crossing time of 9:30 am LT.

### 108 **2.1 MOPITT**

109 MOPITT Version 8 and Version 9 (V8 and V9) Level 1 (L1) and Level 2 (L2) TIR products  
110 are used in this study. L1 data corresponds to all of the radiance observations that are obtained in  
111 MOPITT swaths. They are used subsequently as input to the algorithms that retrieve the CO ver-  
112 tical profiles and total column (TC) amounts, which are referred to as L2 data. The MOPITT L2  
113 products that are utilized here are the CO total column (TC) abundances and two cloud diagnostics  
114 contained in the MOPITT L2 files: the MOPITT cloud description index and the MODIS cloud  
115 diagnostics vector.

116

### 117 **2.2 MODIS**

118 The MODIS products used in this study are the Collection-6 1-km cloud mask (MOD35)  
119 and the cloud height 5-km resolution (MOD06) data. MODIS measures radiances at 36 wave-  
120 lengths, including infrared and visible bands with spatial resolution from 250 m to 1 km. The  
121 MODIS cloud mask algorithm uses up to 19 MODIS spectral bands for better cloud detection  
122 (Ackerman et al., 2008, 1998). The MODIS cloud height is derived using 5 thermal infrared bands  
123 (both day and night) at 5 km spatial resolution.

124

## 125           **2.3 IASI-A**

126           IASI-A is a Fourier Transform Spectrometer on the European space agency (EPS)/MetOp-A  
127 satellite launched in 2006 with a spectral coverage range from 3.62 to 15.5  $\mu\text{m}$  (645 to 2760  $\text{cm}^{-1}$ )  
128 including the CO 2140  $\text{cm}^{-1}$  TIR band. It views the ground through a cross-track rotary scan mirror  
129 with a horizontal resolution of 12 km diameter at nadir, which increases at the larger viewing  
130 angles. The width of the swath is  $\sim$  2200 km with a total of 120 views. The IASI instrument takes  
131 measurements day and night which gives a global coverage twice a day with some gaps between  
132 orbits around the equator. However, clouds in the field of view can obstruct the measurements and  
133 hence reduce the number of the observations (Clerbaux et al., 2009). This study used L2 IASI-A  
134 CO TC values that were retrieved by LATMOS (Laboratoire Atmosphères, Milieux, Observations  
135 Spatiales) using a retrieval code, FORLI (Fast Optimal Retrievals on Layers for IASI), developed  
136 at ULB (Université Libre de Bruxelles) (<https://iasi.aeris-data.fr/co/>). Data are retrieved for a  
137 cloud fraction of less than 25 % (Clerbaux et al., 2009).

## 138           **3. MOPITT cloud detection scheme**

139           The MOPITT retrieval algorithm only performs retrievals in clear-sky conditions. The  
140 MOPITT procedures for identifying clear-sky retrievals from cloud-contaminated pixels involves  
141 a threshold method that makes use of two independent tests, (1) a MOPITT radiance ratio threshold  
142 and (2) a MODIS cloud mask threshold within the MOPITT field of view (Warner et al., 2001,  
143 Deeter, 2011), which are described below.

144

145           **MOPITT radiance threshold.** Radiance from the MOPITT 4.7  $\mu\text{m}$  thermal channel radiance is  
146 compared to the a priori clear-sky radiance calculated by The MOPITT Operational Fast Forward  
147 Model (MOPFAS) (Edwards et al., 1999) for each pixel. If the measured/calculated radiance ratio  
148 is  $\geq 1.0$  for V8 and V9 and  $\geq 0.955$  for other versions (V7 and before), then the observation is  
149 considered “clear”. For this test however, the threshold value may be exceeded under temperature  
150 inversion conditions where clouds are warmer than the underlying surface. This threshold method  
151 is not applicable to polar regions due to the frequent temperature inversions at night, and to avoid  
152 the effect of possible snow and ice coverage on the daytime signals (Warner et al., 2001).

153           **The MODIS Cloud threshold.** The MODIS swath (2330 km) is much wider than the MOPITT  
154 swath (640 km), so it provides complete overlap for MOPITT passes. The MODIS cloud mask

155 (MOD35 L2) product (Ackerman et al., 2008) that is used here has 1 km horizontal resolution at  
156 nadir (Ackerman *et al.*, 1998). Therefore, each MOPITT pixel can encompass  $\sim 480$  MODIS 1  
157 x 1 km pixels. After co-location, relevant MODIS cloud mask parameters of the MODIS are gath-  
158 ered and averaged for each MOPITT pixel. MOD35\_L2, containing data collected from the Terra  
159 platform is used to get the cloud count at each MOPITT pixel and If the MODIS cloud percent is  
160 less than 5%, then the MOPITT pixel is considered clear.

161 In the previous MOPITT products (V8 and before), the MODIS test value supersedes the  
162 MOPITT value over land, i.e., if the MODIS test is “clear” and the MOPITT test is “cloudy”, then  
163 the MOPITT pixel will be considered “clear” (Warner et al., 2001, Marey et al., 2018). However,  
164 if the MOPITT test identifies the pixel as clear and the MODIS test identifies the pixel as cloudy,  
165 then a low cloud test is done. The low cloud test exploits the MODIS IR and visible reflectance  
166 (Warner et al., 2001; Deeter et al., 2017). To assign low clouds for daytime observations, an aver-  
167 aged MODIS IR threshold test value should be  $\geq 0.9$  and an averaged MODIS visible reflectance  
168 test value should be  $\leq 0.95$ . For nighttime observations, a MODIS IR temperature difference test  
169 value  $\geq 0.9$  is interpreted as low clouds (Warner et al., 2001, Marey et al., 2018). While for ocean  
170 scenes even if the low cloud test did not pass, the pixel is considered clear based on either the  
171 MOPITT or MODIS test result (Deeter et al., 2017).

172 For the V9 product, the modified cloud detection algorithm (Deeter et al., 2021) allows CO  
173 retrievals over land when the MOPITT radiance ratio test indicates the pixel is clear although the  
174 MODIS cloud mask test assigns the pixel as cloudy. Hence, a cloud index value of 6 (Table 1) is  
175 now applied for both ocean and land areas (Deeter et al., 2017 and 2021).

176 The final clear/cloudy decision for each MOPITT pixel is based on set of rules summarized  
177 in six cloud indices as follows: The pixel is assigned to be clear and hence retrieved if:

- 178 1: MODIS data are missing but the MOPITT radiance threshold is passed (rare).
- 179 2: MODIS data are clear and the MOPITT radiance threshold is passed. (most confidently clear)
- 180 3: MODIS data are clear but MOPITT radiance threshold is failed. The MODIS result overrides  
181 the MOPITT result.
- 182 4: MODIS data are cloudy but the MOPITT radiance threshold is passed. In this case, the MODIS  
183 low cloud test is applied and in the case of a low cloud, the pixel is treated as clear (occurs mostly  
184 over ocean scenes).
- 185 5: Polar regions only ( $> 65^\circ$  N or S latitude): MODIS data are clear. MOPITT test is not used.

186 6: Ocean and land scenes for V9 no MODIS low cloud: MODIS data are cloudy and the  
 187 MOPITT radiance threshold is passed. This was introduced in V7 for ocean scenes to correct for  
 188 an observed degradation in MODIS cloud products (Moeller and Frey, 2017).

189 If the pixel does not pass any of these tests, then no retrieval is performed. The six cloud  
 190 indices are reported in Level 2 MOPITT files in the “Cloud Description” diagnostic as presented  
 191 in Table 1.

192

193 Table 1. MOPITT Cloud Descriptor Values in L2 CO retrievals

Descriptor value	MOPITT assignment	MODIS assignment	Notes
1	clear	missing	MODIS data are not available
2	clear	clear	
3	cloudy	clear	
4	clear	cloudy, low clouds	
5	Not used	clear	Used only in polar regions
6	clear	cloudy, no low clouds	Introduced in MOPITT V7, for ocean observations only

194

195

## 196 4. Results and Discussion

197

### 198 4.1 Assessment of the successful MOPITT CO retrievals

199 To assess the successful MOPITT CO retrievals in terms of data coverage, the statistics of  
 200 the L2 data from 2000 to 2020 for V9 and V8 are computed. Buchholz et al. (2017) recommended  
 201 avoiding the use of MOPITT above 60°N as the sea ice may not be correctly accounted for in the  
 202 retrievals. The fraction of daily valid data between 90°S–90°N and 60°S–60°N (for land and ocean  
 203 combined) are shown in Figure 1. The successful rate is calculated by taking the ratio of the num-  
 204 ber of daily CO data retrievals (L2) to the total number of daily radiance measurements (L1). For

205 the 90°S–90°N, the successful retrieval rate of V8 and V9 varies between 27%–33% and 35%–  
206 40%, respectively. While the 60°S–60°N domain has a successful retrieval rate between 34%–  
207 42% and 40%–50%, for V8 and V9 respectively. Therefore, the number of daytime V9 MOPITT  
208 retrievals has increased by 15-20% for 90°S–90°N and 60°S–60°N relative to Version 8 product.  
209 However, the gain in data coverage varies significantly on spatial level.

210 Figure 2 shows the spatial coverage rate per day (the fraction of the successful retrievals, L2  
211 to the total number of radiance measurements, L1) using 2014 as a representative year gridded in  
212  $1^\circ \times 1^\circ$  bins. It is apparent that some regions exhibit high coverage rates (close to 100%) in all  
213 seasons, such as northern Africa for both V8 and V9, so there are no added observations over such  
214 regions as it is indicated by the middle panel (V9-V8). While other regions exhibit large gain in  
215 retrievals compared to V8 product which varies seasonally. For example, in Canada, the data cov-  
216 erage of V8 (right panel) reached 50% in summer (e.g. Hudson Bay), but drops to less than 10%  
217 in winter due to high cloud cover. Interestingly, V9 successful retrievals (left panel) for Canada  
218 demonstrated significant data enhancement, especially in winter where observations in some areas  
219 has doubled relative to V8 as shown in the top panel of Figure 2. Additionally, the Amazon region  
220 experienced significant data increase compared to V8, especially in JJA months. The increase in  
221 retrieval yield over the Amazon region has been investigated in more details by Deeter et al.  
222 (2021).

223 Here we focus on daytime data, and therefore there is a cut off at high northern latitudes in  
224 the northern-hemisphere winter, and at high southern latitudes in the southern-hemisphere winter.  
225 In general, high latitude regions (poleward of 65°) have strong seasonal variations in data cover-  
226 age, with the northern high latitudes showing the highest coverage rates for both V9 and V8 in  
227 June, July, and August, and the southern high latitudes exhibiting the highest rates in December,  
228 January, and February as a result of less cloud in the summer. However, V9 successful retrievals  
229 of spring (February, March, and April) and fall (September, October and November) seasons ex-  
230 perience a significant coverage gain in comparison to V8. Hence, the cloud detection scheme  
231 modifications in the new V9 product resulted in an improvement in observational coverage, espe-  
232 cially over land (Deeter et al., 2021).

233  
234

## 235           **4.2 Analysis of standard and non-standard MOPITT product**

236           In this section, we present an analysis of Moderate Resolution Imaging Spectroradiometer  
237 (MODIS) cloud heights and cloud mask products along with MOPITT retrieval cloud flag de-  
238 scriptors to understand the impact of cloud conditions on the MOPITT observational coverage,  
239 with a particular focus on observations over Canada.

240           CO TC were retrieved for a selected number of dates and locations by suppressing the cloud  
241 detection scheme, so that all MOPITT L1 data were used to produce the L2 product regardless of  
242 the cloud conditions. This non-cloud masked product will be referred to here as the non-standard  
243 product. Analysis of the CO TC V8 L2 standard (cloud filtered) and non-standard product (non-  
244 cloud masked) were performed for some selected cases. Figures 6a and 6b show the standard and  
245 non-standard CO product on 16 August 2018, respectively, over the region between 78°W–92°W  
246 and 44°N–60°N, which covers Ontario, Canada, near Hudson Bay. The standard (cloud masked)  
247 product indicates that about 60% of the data are missing. Comparing it to the non-standard (non-  
248 masked) product, some features can be observed in the non-standard product over the regions that  
249 were missing data in the V8 standard product. A coherent structure is present between 50°N–54°N  
250 (as it is indicated by pink and purple colors). The IASI TC for the same area and time was analyzed  
251 to corroborate whether the features in the non-cloud-masked product are actual CO plumes  
252 (Figures 6c). Comparing IASI CO TC on 16 August 2018 (Figures 6c) to the corresponding  
253 MOPITT (Figure 6b) illustrate a strong CO plume around 50-55 °N and -94: -84 °W that is  
254 apparent in both IASI and MOPITT. In the next section the MODIS cloud height product was used  
255 to diagnose the cause of the missing (not retrieved in the V8 standard product) CO features.

## 256           **4.3 Regional analysis of MODIS cloud height and MOPITT data**

257           Figures 6d depicts the V8 MOPITT cloud index (see Table 1), for the case on 16 August  
258 2018. Retrievals were assigned cloud index 2 (MODIS and MOPITT clear, grey color), 3 (MODIS  
259 clear and MOPITT cloudy, dark blue), and 4 (low clouds, cyan color). Figures 6d shows that the  
260 V8 L2 data on 16 August 2018 case were retrieved based on clear and low cloud conditions as  
261 indicated by flag number 2 and flag number 4. Figure 6e displays the MODIS cloud height (and  
262 cloud mask for the same swath on 16 August 2018. Comparing the low cloud retrieval area (cyan  
263 color) to the corresponding MODIS cloud height (Fig. 6e) and cloud mask (Figure 6f), it can be

264 seen that this area has cloud percent (the term “cloud” encompasses water clouds and aerosols) by  
265 more than 90% and has cloud heights less than 1 km, as illustrated by the grey color (Figure 6e).  
266 The MODIS cloud height also shows other areas that have low clouds (grey and blue colors) where  
267 there were no retrievals in the V8 standard product. Those pixels collocate with the coherent  
268 pattern region (between 52°N–54°N) that were shown in the non-masked product (Figure 6b).  
269 Therefore, it appears that some of the potential retrievals were missed in the V8 standard retrieval  
270 due to misidentification of low cloud pixels. It is necessary to examine additional cases using the  
271 same approach to determine whether these findings are widespread.

272

#### 273 **4.4 Analysis of V8 cases under different cloud and pollution conditions**

274 In this section, additional cases are investigated by analyzing the cloud filtered (V8 standard)  
275 and the non-cloud masked, along with the MODIS cloud height and cloud mask products. Figure  
276 7 shows the results over Canada, on 12 April 2010 and it indicates that, about 70% of the data are  
277 missing in the standard retrievals (Figure 7a). However, the non-cloud masked product (Figure 7b)  
278 captures notable features between 54°N–56°N and 90°W–98°W (as indicated by the red colors in  
279 Figure 7b). The MOPITT cloud flag description on 12 April 2010 (Figure 7d) reveals that all L2  
280 data were retrieved under clear conditions (MODIS cloud percent less than 5%) as indicated by  
281 the flag number 2 (grey color) and the MOPITT diagnostics data (Figure 7c). However, the  
282 corresponding MODIS cloud height (Figure 7e) showed an area of very low cloud heights that are  
283 less than 500 m (around 54°N–56°N), where the MOPITT measurements were not retrieved  
284 completely in the V8 standard product as they were considered cloudy (with more than 5% cloud  
285 cover, see Figure 7f). Comparing this area to the collocated non-masked CO product (Figure 7b),  
286 it can be noted that it exactly matches the coherent pattern that was observed between 54°N–56°N.  
287 Looking to IASI CO TC for the same time and location on 12 April 2010 (Figures 7c), it can be  
288 seen that most of the CO features in the area of 52-56 latitude and -100: -92 longitudes (Figure 7b)  
289 are not captured as well due to their cloud detection scheme.

290 An unusually active forest fire season occurred in the vicinity of Fort McMurray, Alberta, in  
291 May 2016. Figures 8a and 8b display the V8 standard and non-standard CO TC on 6 May (day),  
292 respectively. Again, the non-standard CO product exhibits a notable coherent pattern over some  
293 areas that were not retrieved in the standard product. On 6 May 2016, there is a CO plume around



294 50°N–52°N and 108°W–112°W longitude that is indicated by the purple colors (Figure 8b) and it  
295 is completely missed in the V8 standard product. On the other hand, IASI shows a consistency  
296 with the non-masked MOPITT product where a prominent CO plumes was observed around 50-  
297 56 latitude and -112: -104 longitudes which coincide the corresponding MOPITT (Figure 8b).

298 The elevated CO values on 6 May 2016 is likely to be a result of Fort McMurray fire  
299 emissions in northern Alberta (as indicated by MODIS fire images, not shown). Considering the  
300 low cloud detection during the Fort McMurray fires, the MODIS cloud height data of the  
301 corresponding MOPITT pixels on 6 May 2016 (Figure 8e) suggest that none of the low cloud (blue  
302 colors) pixels were retrieved in the standard product as it is implied by the MOPITT flag number  
303 (Figure 8d) (all values are 2).

304

#### 305 **4.5 MODIS height comparison with MOPITT radiance ratio**

306

307 As it is mentioned in section 3 the MOPITT retrieval algorithm only retrieve CO in clear-  
308 sky conditions. The cloud detection scheme utilizes information from both MODIS cloud mask  
309 product and the MOPITT’s thermal-channel radiances (Warner et al., 2001). Radiance from the  
310 MOPITT 4.7  $\mu\text{m}$  thermal channel radiance is compared to the calculated model for each pixel. If  
311 the measured/calculated radiance ratio is greater than the threshold (which is one for V8), then the  
312 observation is considered “clear”.

313 In MOPITT V8 and before, the MODIS test value supersedes the MOPITT test value over  
314 land, i.e., the MOPITT pixel will be considered “clear” if the MODIS test is “clear” and the  
315 MOPITT test is “cloudy”. However, the MOPITT pixel will be considered “cloudy” if the  
316 MOPITT test identifies the pixel as clear and the MODIS test identifies the pixel as cloudy. Hence  
317 V8 level 2 retrievals are processed over land just if the MODIS test passes. For the MOPITT V9  
318 product, Deeter et al., (2021) modified the cloud detection algorithm by allowing CO retrievals  
319 when the MOPITT radiance ratio (MRT) test indicates the pixel is clear although the MODIS cloud  
320 mask test assigns the pixel as cloudy. Deeter et al., (2021) modified the cloud detection algorithm  
321 by allowing CO retrievals when the MOPITT radiance ratio test indicates the pixel is clear alt-  
322 hough the MODIS cloud mask test assigns the pixel as cloudy.

323 To understand how the new V9 cloud detection scheme improved the coverage rate, an anal-  
324 ysis of the MRT and MODIS cloud height has been conducted for many cases over Canada. The  
325 data on 6 May 2016 are presented here as a case study and are shown in Figure 9. It can be seen  
326 that there is a negative correlation between the MRT and MODIS cloud height with a slope of -  
327 0.06 and a correlation of  $R = 0.68$ .

328 A Box and Whisker plot of MRT and the corresponding MODIS cloud heights for various  
329 groups are displayed in Figure 9b. Since the modified cloud detection scheme of V9 relies on the  
330 MRT threshold test (the threshold value is one), It is expected that, most of the observations with  
331 cloud heights up to 3 km are incorporated in V9 retrievals as illustrated Figure 9b.

332 Figures 9c and d in the bottom panel depict the histograms density of MODIS cloud heights of  
333 the corresponding MOPITT clear/MODIS clear observations and MOPITT clear/MODIS cloudy,  
334 respectively on 6 May 2016. The successful retrievals using MOPITT clear/MODIS clear pixels  
335 and MOPITT clear/MODIS cloudy are 45.4%, and 14.2%, respectively.

336 Since MRT correlates negatively with the low cloud heights (as indicated above in Figure 9a),  
337 the low cloud cases are included in V9 (Figure 9d) with high proportion of heights less than 3 km.  
338 Hence, adding low cloud observations as a result of considering MRT values of greater than 1  
339 enhances the MOPITT coverage percentage by 14.2% compared to 45.4% successful retrievals  
340 without considering the low cloud cases. The total coverage rate is about 60% with about a 30%  
341 (14.2/45.4) gain in data coverage. Therefore, using the MRT cloud test independently in V9 cloud  
342 detection scheme resolved the problem of low cloud miss-detection over land, which results in a  
343 significant data coverage increase, especially over the Canada region.

344

#### 345 **4.6 MOPITT and IASI comparison**

346 We examine the impact of the increased observational coverage in the MOPITT TIR V9  
347 product in comparison to IASI data over Canada for three case studies. The first and third cases  
348 are associated with biomass burning emissions (6 May 2016 and 16 August 2018), while the se-  
349 cond case represents typical conditions with no extreme air pollution (12 April 2010). Figure 10  
350 shows maps of 1-day/morning overpasses of CO total columns measured by MOPITT and IASI  
351 on 6 May 2016. Figures 10a and 7b show MOPITT V9 and V8 data, respectively, while Figures  
352 10c and 7d show the corresponding IASI data (collocated with MOPITT) and the entire IASI CO  
353 field (gridded in  $0.25^\circ \times 0.25^\circ$  bins), respectively. As seen in Figures 10a and 10b, there is a gap

354 with missing MOPITT data in V8 that extends across Alberta and Saskatchewan between 110°W  
355 and 100°W, but the data are present in V9 as a result of the improved retrievals in low cloud  
356 conditions (as indicated by the MODIS cloud heights in Figure 8e). The high CO total column  
357 values that are added in MOPITT V9 product coincide with the high AOD and OMI UV Aerosol  
358 Index (UVAI) values (not shown) from the Fort McMurray fire emissions. Smoke was transported  
359 from the eastern part of Alberta, moving into Saskatchewan and central Alberta in the vicinity of  
360 the high CO values. Interestingly, the added retrievals in V9 exhibit a pattern that is consistent  
361 with the IASI data (Figure 10c). Since IASI has daily global coverage compared to MOPITT's 3-  
362 day global coverage, the entire smoke plume is captured by IASI (Figure 10d).

363 Figure 11 depicts the scatter plots of IASI and MOPITT TIR V9 and V8 retrievals over  
364 Canada on 6 May 2016 and for the entire month of May 2016 (monthly average). IASI and  
365 MOPITT data are gridded in 0.25x0.25 deg., then the daily collocated data are selected for the  
366 analysis.

367 In general, IASI and MOPITT retrievals are consistent to a large extent with a correlation  
368 coefficient of 0.98-0.99 and 0.97-0.98 for V8 and V9, respectively. However, IASI has higher  
369 values than MOPITT over Canada, with the slope varying from 1.04 to 1.06. Total CO column  
370 biases for V9 are somewhat larger than for V8 products; with a slope for V9 of 1.05 and 1.06,  
371 whereas for V8 it is 1.04 and 1.05 for data on 6 May 2016 and for all of May 2016, respectively.  
372 These discrepancies occur at high CO values, and since the added data in V9 are mainly in heavily  
373 polluted regions, the IASI bias is greater for V9 than V8.

374 For the second case analysis on 12 April 2010, V9 (shown in Figure 12a) exhibited greater  
375 data coverage relative to V8 (Figure 12b) around 126°W, 56-60°N, 90°W, 56-60°N, and 80°W,  
376 44°N as a result of retrievals of low cloud height pixels (Figure 7e). Figure 12c shows generally  
377 good agreement between IASI CO total column values and corresponding MOPITT retrievals. As  
378 this time of year has no extreme air pollution sources (such as forest fire emissions), the CO total  
379 column values over land are in the range of 20-30  $10^{17}$  molecules/cm<sup>2</sup>, which can be seen in the  
380 whole IASI CO total column field in Figure 12d. Consequently, as shown in Figure 13, the IASI  
381 biases with MOPITT V8 and V9 are generally similar, with comparable correlations and slopes.

382 Comparison of MOPITT V9 and V8 on 16 August 2018 over Canada, in Figure 14, shows the  
383 greater number of successful MOPITT retrievals in V9 that were discarded in V8. The added data  
384 in V9 are around 80°W-90°W, and 50°N-56°N and 100°W-117°W, 54°N-56°N. Those regions are

385 associated with cloudy areas of relatively low cloud heights as indicated by the MODIS cloud  
386 mask and height (Figure 6e and 6f). As shown in Figure 14c, the IASI observational pattern is  
387 generally consistent with the corresponding MOPITT CO total columns. However, there is an ap-  
388 parent positive IASI bias around 80°W-90°W and 54°N where IASI CO values exceed  $50 \times 10^{17}$   
389 molecules/cm<sup>2</sup> compared to  $30 \times 10^{17}$  molecules/cm<sup>2</sup> for MOPITT. These high CO values are as-  
390 sociated with the dense pollution plume that extends across Canada as shown in the map in Figure  
391 14d with the whole IASI observational scene and in Figure 15a with the MODIS Terra image  
392 overlaid with the thermal anomaly spots.

393 The scatterplots of CO total column values between IASI and MOPITT TIR V9 and V8 for  
394 August 2018 are shown in Figure 15b. The slopes of the relationship between IASI and MOPITT  
395 V8 data on 16 August 2016 and for all of August are 1.09 and 1.07, respectively. Since the added  
396 MOPITT retrievals in V9 are associated with higher CO total column values, the slopes increase  
397 to 1.12 and 1.1, respectively, with smaller correlation coefficients. CALIPSO total attenuated  
398 backscatter at 532 nm on 16 Aug. 2018 for the two yellow swaths shown in Figure 15a are pre-  
399 sented in Figures 15c and 15d. The smoke aerosols were observed at altitudes between 2 km and  
400 6 km, as measured by CALIPSO, indicating that convective lofting may have elevated the fire  
401 emissions above the boundary layer into the free troposphere. The large CO enhancements ob-  
402 served by IASI around -80°W-90°W and 54°N (Figure 14c) are collocated with the maximum  
403 aerosol backscatter coefficient at ~3 km detected by the CALIPSO lidar (Figure 15d). However,  
404 CO in this area is underestimated by MOPITT TIR relative to IASI (Figure 14b) resulting in 12%  
405 overall bias over Canada on 16 August 2018 (as indicated by the slope of 1.12).

406 Similar results were found by Turquety et al. (2009) as their study revealed that IASI CO is on  
407 average 35% higher than MOPITT in regions of elevated CO concentrations during extreme fire  
408 events. There are many factors that could explain the discrepancies between IASI and MOPITT  
409 during pollution events. One of them is the different horizontal resolution of the two instruments  
410 ( $22 \text{ km} \times 22 \text{ km}$  for MOPITT and a 12-km diameter for IASI), especially above inhomogeneous  
411 scenes. A second major factor that could contribute to the differences between the MOPITT and  
412 IASI retrievals is the a priori used in the retrievals. IASI uses a fixed a priori while MOPITT has  
413 variable a priori profiles. George et al. (2015) examined the impact of the a priori on the IASI and  
414 MOPITT data and found that using the same a priori constraints slightly improved the correlation  
415 between the two data sets and reduced the large discrepancies (total column biases over 15 %)

416 observed at some places by a factor of 2 to 2.5. However, other regions did not show any bias  
417 reduction. A third factor is the difference in vertical sensitivity between the two instruments, as  
418 reflected by their averaging kernel matrices (the sensitivity of the retrieval to the abundance of CO  
419 at different altitudes). The instruments have different degrees of freedom for signal (DOFS), which  
420 is given by the trace of the averaging kernel matrix; the DOFS of the MOPITT retrievals is lower  
421 than the corresponding IASI retrievals (not shown). Although both instruments in general have  
422 good sensitivity in the middle troposphere, IASI's averaging kernel indicating greater sensitivity  
423 in the upper troposphere as well. The difference in averaging kernels for the instruments can be  
424 attributed to instrumental and retrieval factors (George et al., 2015). For example, surface emis-  
425 sivity and water vapor are treated differently in the two retrieval algorithms. The MOPITT algo-  
426 rithm retrieves emissivity simultaneously with CO but uses a fixed water vapor profile from  
427 NOAA/National Centers for Environmental Prediction (NCEP), while IASI assumes a fixed emis-  
428 sivity but estimates the water vapor amount (Barré, J., et al., 2015). Understanding how the factors  
429 discussed here, as well as others, potentially contribute to the discrepancies between MOPITT and  
430 IASI will be further investigated in future work

431

## 432 **5. Conclusion**

433 In this study, an analysis has been performed to understand the improvements in observa-  
434 tional coverage over Canada in the new MOPITT V9 product. Temporal and spatial analysis of  
435 V9 indicates a general coverage gain of 15-20% relative to V8 which vary regionally and season-  
436 ally. For example, the number of successful MOPITT retrievals in V9 was doubled over Canada  
437 in winter.

438 The standard (cloud filtered) V8 CO TC (L2) product was compared with a non-standard  
439 (non-cloud masked) version of the retrievals for selected days to understand the observation gain  
440 in V9 relative to V8. The results reveal some interesting structures that were observed frequently  
441 in the non-cloud masked product but which were missing in the standard the V8 product. Those  
442 features are not captured in V8 standard product because the cloud detection scheme did not  
443 properly detect many low cloud cases over land.

444 The modified V9 cloud detection scheme utilizes MRT test (threshold value of 1) individu-  
445 ally which allow CO retrievals when the MRT test indicates the pixel is clear although the MODIS

446 cloud mask test assigns the pixel as cloudy. Since MRT correlates negatively with the low cloud  
447 heights, most of low cloud observations (up to 3 km) are included in V9 L2 retrievals. Hence, the  
448 incorporation of the MRT test over land will resolve the low cloud detection issue as it is demon-  
449 strated by MODIS cloud height correlation. Hence, adding low cloud observations as a result of  
450 considering MRT values of greater than 1 enhances the MOPITT coverage percentage.

451

452 The improved V9 cloud detection scheme benefits regions that are often characterized by  
453 high aerosol concentrations (e.g. biomass burning emissions). An analysis of MOPITT and IASI  
454 CO are conducted for three cases. The first and third cases are associated with biomass burning  
455 emissions, while the second case represents typical conditions with no extreme air pollution. The  
456 added retrievals in V9 exhibit a pattern that is generally consistent with the corresponding IASI  
457 data. However, there are IASI MOPITT discrepancies occur at high CO values, and since the added  
458 data in V9 are mainly in heavily polluted regions, the IASI bias is greater for V9 than V8. So, IASI  
459 MOPITT CO TC comparison indicated generally good agreement with about 5-10% positive bias  
460 which increases in highly polluted scenes.

461

462

## 463 **ACKNOWLEDGMENTS**

464 The authors would like to thank the CSA (Canadian Space Agency) for their financial  
465 support of this research. NCAR (National Center for Atmospheric Research) is sponsored by the  
466 National Science Foundation and operated by the University Corporation for Atmospheric  
467 Research. The NCAR MOPITT project is supported by the National Aeronautics and Space  
468 Administration (NASA) Earth Observing System (EOS) Program. The MOPITT team  
469 acknowledges support from the Canadian Space Agency (CSA), the Natural Sciences and  
470 Engineering Research Council (NSERC) and Environment Canada, and the contributions of  
471 COMDEV (the prime contractor) and ABB BOMEM. The authors thank the AERIS infrastructure  
472 (<http://www.aeris-data.fr>) for providing access to the IASI CO data.

473

474

475

476       **6. References**

477

478 Ackerman, S. A., K. I. Stabala, W. P. Menzel, R. A. Frey, C. Moeller, and L. E. Gumley (1998),  
479 Discriminating clear sky from clouds with MODIS, *J. Geophys. Res.*, 103, 32,141 – 32,157,  
480 doi:10.1029/1998JD200032.

481 Ackerman, S. A., R. E. Holz, R. Frey, E. W. Eloranta, B. Maddux, and M. J. McGill (2008), Cloud  
482 detection with MODIS: Part II. Validation, *J. Atmos. Oceanic Technol.*, 25, 1073 – 1086.

483

484 Barré, J., Gaubert, B., Arellano, A. F., Worden, H. M., Edwards, D. P., Deeter, M. N., ... &  
485 Hurtmans, D. (2015). Assessing the impacts of assimilating IASI and MOPITT CO retrievals using  
486 CESM-CAM-chem and DART. *Journal of Geophysical Research: Atmospheres*, 120(19), 10-501.

487

488 Buchholz, R. R., M. N. Deeter, H. M. Worden, J. Gille, D. P. Edwards, J. W. Hannigan, N. B.  
489 Jones, C. Paton-Walsh, D. W. T. Griffith, D. Smale, J. Robinson, K. Strong, S. Conway, R. Suss-  
490 mann, F. Hase, T. Blumenstock, E. Mahieu, and B. Langerock (2017), Validation of MOPITT  
491 carbon monoxide using ground-based Fourier transform infrared spectrometer data from  
492 NDACC, *Atmos. Meas. Tech.*, 10(5), 1927–1956, doi:10.5194/amt-10-1927-2017.

493 Buchholz, R. R., Worden, H. M., Park, M., et al., Air pollution trends measured from Terra: CO  
494 and AOD over industrial, fire-prone, and background regions, *Remote Sensing of Environment*,  
495 256, 112275, doi: 10.1016/j.rse.2020.112275, 2021.

496 Clerbaux, C., Boynard, A., Clarisse, L., George, M., Hadji-Lazaro, J., Herbin, H., ... & Coheur, P.  
497 F. (2009). Monitoring of atmospheric composition using the thermal infrared IASI/MetOp  
498 sounder. *Atmospheric Chemistry and Physics*, 9(16), 6041-6054.

499 Deeter, M. N., Edwards, D. P., Francis, G. L., Gille, J. C., Martínez-Alonso, S., Worden, H. M.,  
500 & Sweeney, C. (2017). A climate-scale satellite record for carbon monoxide: the MOPITT Version  
501 7 product.

502 Deeter, M. N., Emmons, L. K., Francis, G. L., Edwards, D. P., Gille, J. C., Warner, J. X., ... &  
503 Yudin, V. (2003). Operational carbon monoxide retrieval algorithm and selected results for the  
504 MOPITT instrument. *Journal of Geophysical Research: Atmospheres*, 108(D14).

505 Deeter, M. N., Worden, H. M., Gille, J. C., Edwards, D. P., Mao, D., & Drummond, J. R. (2011).  
506 MOPITT multispectral CO retrievals: Origins and effects of geophysical radiance errors. *Journal*  
507 *of Geophysical Research: Atmospheres*, 116(D15).

508

509 Deeter, M. N., Mao, D., Martínez-Alonso, S., Worden, H. M., Andreae, M. O., & Schlager, H.  
510 (2021). Impacts of MOPITT cloud detection revisions on observation frequency and mapping of  
511 highly polluted scenes. *Remote Sensing of Environment*, 262, 112516.

512

513 Drummond, J. R., & Mand, G. S. (1996). The Measurements of Pollution in the Troposphere  
514 (MOPITT) instrument: Overall performance and calibration requirements. *Journal of Atmospheric*  
515 *and Oceanic Technology*, 13(2), 314-320.

516 Drummond, J. R., Zou, J., Nichitiu, F., Kar, J., Deschambaut, R., & Hackett, J. (2010). A review  
517 of 9-year performance and operation of the MOPITT instrument. *Advances in Space Re-*  
518 *search*, 45(6), 760-774.

519 Duncan, B. N., Logan, J. A., Bey, I., Megretskaja, I. A., Yantosca, R. M., Novelli, P. C., ... &  
520 Rinsland, C. P. (2007). Global budget of CO, 1988–1997: Source estimates and validation with a  
521 global model. *Journal of Geophysical Research: Atmospheres*, 112(D22).

522 Edwards, D. P., Halvorson, C. M., & Gille, J. C. (1999). Radiative transfer modeling for the EOS  
523 Terra satellite Measurement of Pollution in the Troposphere (MOPITT) instrument. *Journal of*  
524 *Geophysical Research: Atmospheres*, 104(D14), 16755-16775

525 Edwards, D. P., Emmons, L. K., Gille, J. C., Chu, A., Attié, J. L., Giglio, L., ... & Ziskin, D. C.  
526 (2006). Satellite-observed pollution from Southern Hemisphere biomass burning. *Journal of Geo-*  
527 *physical Research: Atmospheres*, 111(D14).

528 George, M., Clerbaux, C., Bouarar, I., Coheur, P. F., Deeter, M. N., Edwards, D. P., ... & Worden,  
529 H. M. (2015). An examination of the long-term CO records from MOPITT and IASI: comparison  
530 of retrieval methodology. *Atmospheric Measurement Techniques*, 8(10), 4313-4328.

531 Jiang, Z., Jones, D. B., Kopacz, M., Liu, J., Henze, D. K., & Heald, C. (2011). Quantifying the  
532 impact of model errors on top-down estimates of carbon monoxide emissions using satellite ob-  
533 servations. *Journal of Geophysical Research: Atmospheres*, 116(D15).

534 Kulawik, S. S., J. Worden, A. Eldering, K. Bowman, M. Gunson, G. B. Osterman, L. Zhang, S.  
535 Clough, M. W. Shephard, and R. Beer (2006), Implementation of cloud retrievals for Tropospheric



536 Emission Spectrometer (TES) atmospheric retrievals: part 1. Description and characterization of  
537 errors on trace gas retrievals, *J. Geophys. Res.*, 111, D24204, doi:10.1029/2005JD006733.

538 Landgraf, J., aan de Brugh, J., Scheepmaker, R., Borsdorff, T., Hu, H., Houweling, S., Butz, A.,  
539 Aben, I., and Hasekamp, O.: Carbon monoxide total column retrievals from TROPOMI shortwave  
540 infrared measurements, *Atmos. Meas. Tech.*, 9, 4955–4975, [https://doi.org/10.5194/amt-9-4955-](https://doi.org/10.5194/amt-9-4955-2016)  
541 [2016](https://doi.org/10.5194/amt-9-4955-2016), 2016.

542

543 Li, J., Liu, C. Y., Huang, H. L., Schmit, T. J., Wu, X., Menzel, W. P., & Gurka, J. J. (2005). Optimal  
544 cloud-clearing for AIRS radiances using MODIS. *IEEE Transactions on Geoscience and Remote*  
545 *Sensing*, 43(6), 1266-1278.

546 Marey H., Drummond J., (2018). Analysis of MOPITT Cloud-Clearing Algorithm V3-V7. Internal  
547 report for “MOPITT Data Enhancements through Improved Cloud Clearing “project.

548

549 Moeller, C. and Frey, R.: Terra MODIS Collection 6.1 Calibration and Cloud Product Changes,  
550 Version 1.0, available at: [https://modis-atmosphere.gsfc.nasa.gov/sites/default/files/Mod-](https://modis-atmosphere.gsfc.nasa.gov/sites/default/files/ModAtmo/C6.1_Calibration_and_Cloud_Product_Changes_UW_frey_CCM_1.pdf)  
551 [dAtmo/C6.1\\_Calibration\\_and\\_Cloud\\_Product\\_Changes\\_UW\\_frey\\_CCM\\_1.pdf](https://modis-atmosphere.gsfc.nasa.gov/sites/default/files/ModAtmo/C6.1_Calibration_and_Cloud_Product_Changes_UW_frey_CCM_1.pdf) (last access: 16  
552 March 2021), 2017.

553 Turquety, S., Hurtmans, D., Hadji-Lazaro, J., Coheur, P. F., Clerbaux, C., Josset, D., & Tsamalis,  
554 C. (2009). Tracking the emission and transport of pollution from wildfires using the IASI CO  
555 retrievals: analysis of the summer 2007 Greek fires. *Atmospheric Chemistry and Physics*, 9(14),  
556 4897-4913.

557 Spivakovsky, C. M., Logan, J. A., Montzka, S. A., Balkanski, Y. J., Foreman-Fowler, M., Jones,  
558 D. B. A., ... & Wofsy, S. C. (2000). Three-dimensional climatological distribution of tropospheric  
559 OH: Update and evaluation. *Journal of Geophysical Research: Atmospheres*, 105(D7), 8931-8980.

560 Strode, S. A., & Pawson, S. (2013). Detection of carbon monoxide trends in the presence of inter-  
561 annual variability. *Journal of Geophysical Research: Atmospheres*, 118(21), 12-257.

562 Susskind, J., Barnet, C. D., & Blaisdell, J. M. (2003). Retrieval of atmospheric and surface param-  
563 eters from AIRS/AMSU/HSB data in the presence of clouds. *IEEE Transactions on Geoscience*  
564 *and Remote Sensing*, 41(2), 390-409.

565 Vidot, J., Landgraf, J., Hasekamp, O. P., Butz, A., Galli, A., Tol, P., & Aben, I. (2012). Carbon  
566 monoxide from shortwave infrared reflectance measurements: A new retrieval approach for clear  
567 sky and partially cloudy atmospheres. *Remote sensing of environment*, 120, 255-266.

568 Warner, J. X., Gille, J. C., Edwards, D. P., Ziskin, D. C., Smith, M. W., Bailey, P. L., & Rokke,  
569 L. (2001). Cloud detection and clearing for the Earth Observing System Terra satellite Measure-  
570 ments of Pollution in the Troposphere (MOPITT) experiment. *Applied Optics*, 40(8), 1269-1284.

571 Worden, H. M., Deeter, M. N., Frankenberg, C., George, M., Nichitiu, F., Worden, J., ... & De  
572 Laat, A. T. J. (2013). Decadal record of satellite carbon monoxide observations. *Atmospheric*  
573 *Chemistry and Physics*, 13(2), 837-85.

574

575

576

577

578

579

580

581

582

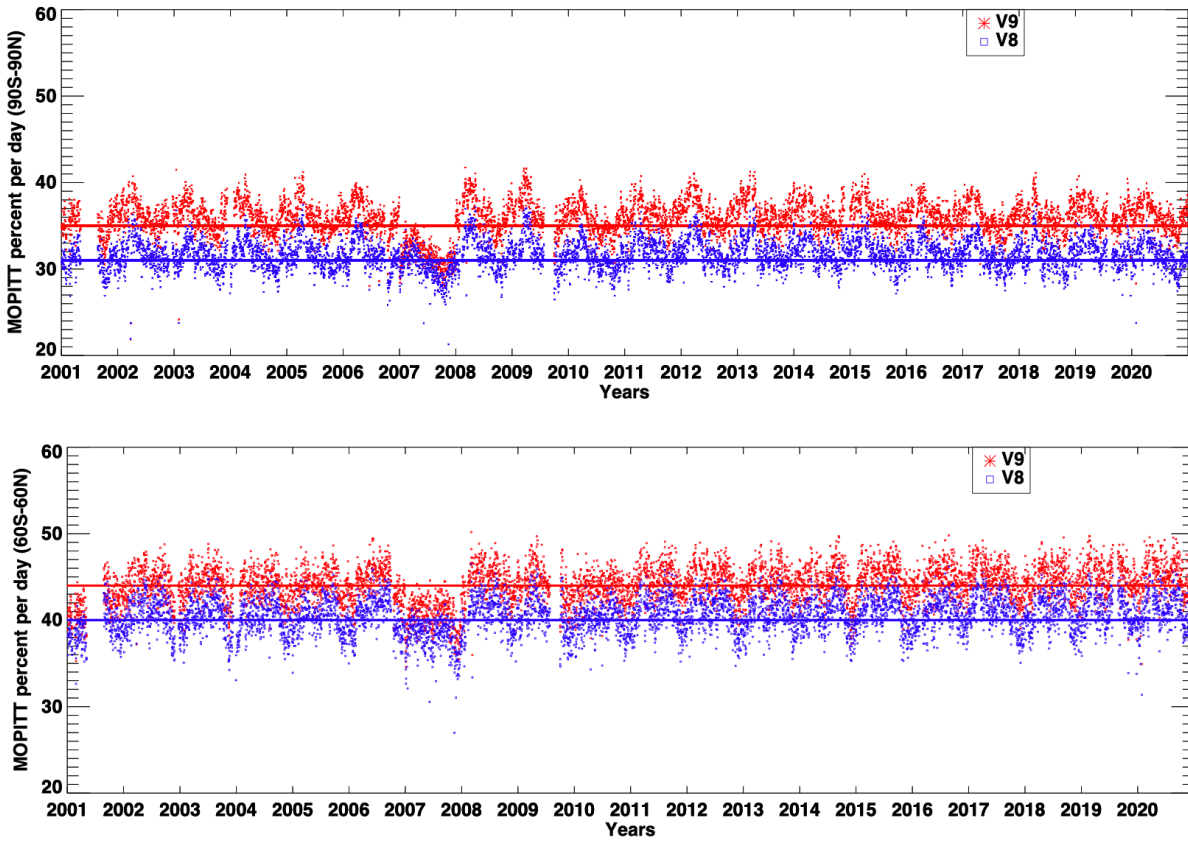
583

584

585

586

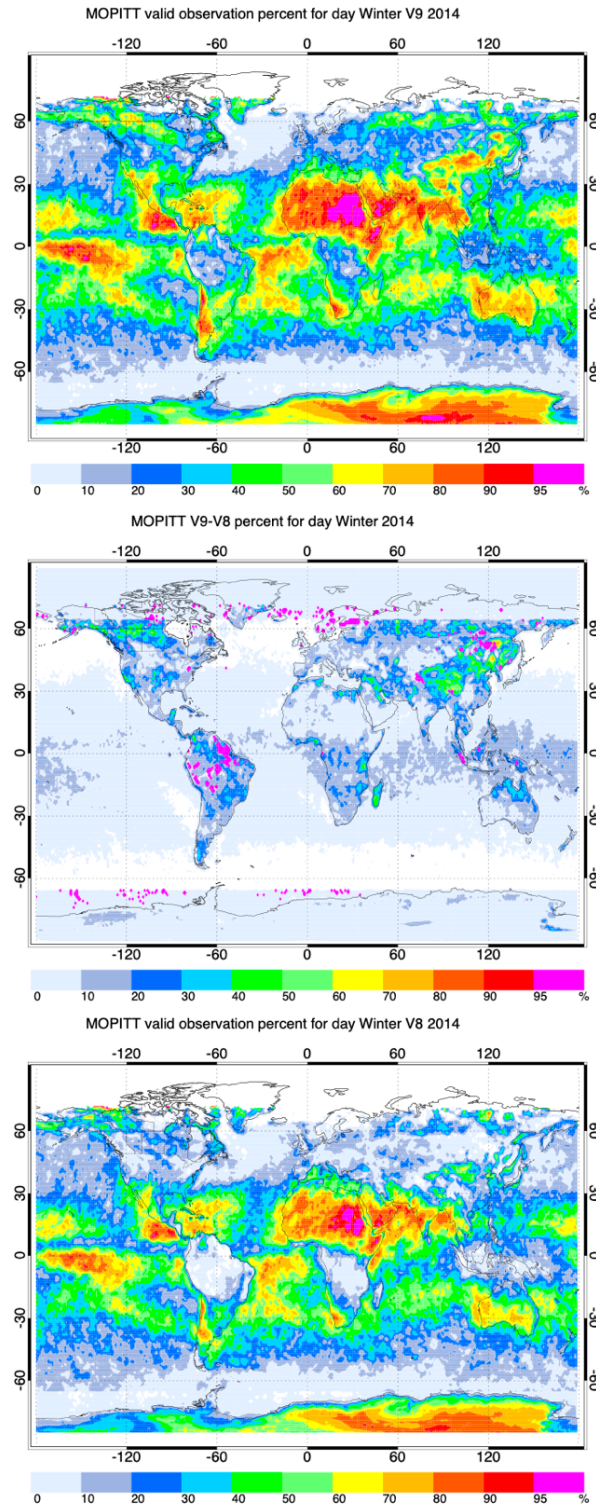
587



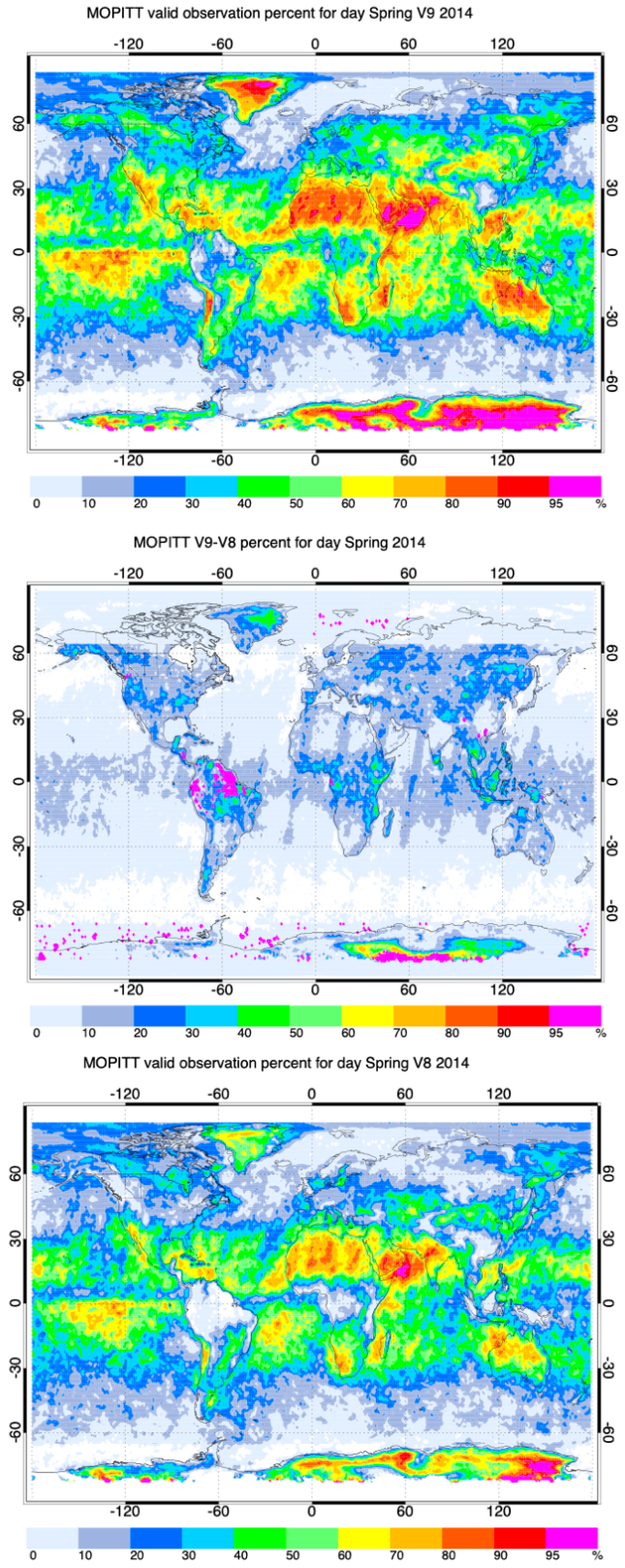
588

589

590 Figure (1) The percentage of successful daily MOPITT retrievals between 90°S–90°N and 60°S–  
591 60°N from 2000 to 2020 for V9 and V8. The solid lines represent the average successful retrieval  
592 for the entire period.



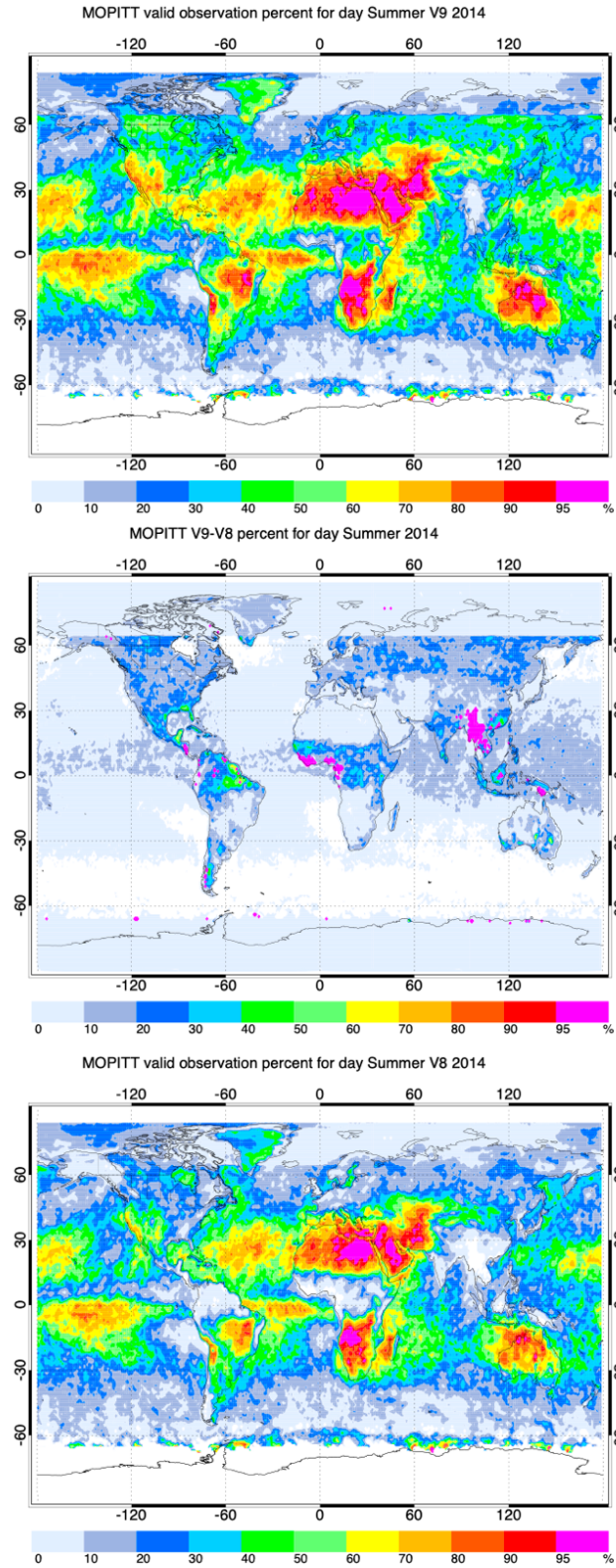
593  
 594 Figure (2) Seasonally averaged spatial distribution of the successful MOPITT retrievals in winter  
 595 2014 for V9 (left panel), V8 (right panel) and V9-V8 (middle panel). Data were aggregated into  
 596  $1^\circ \times 1^\circ$  bins.



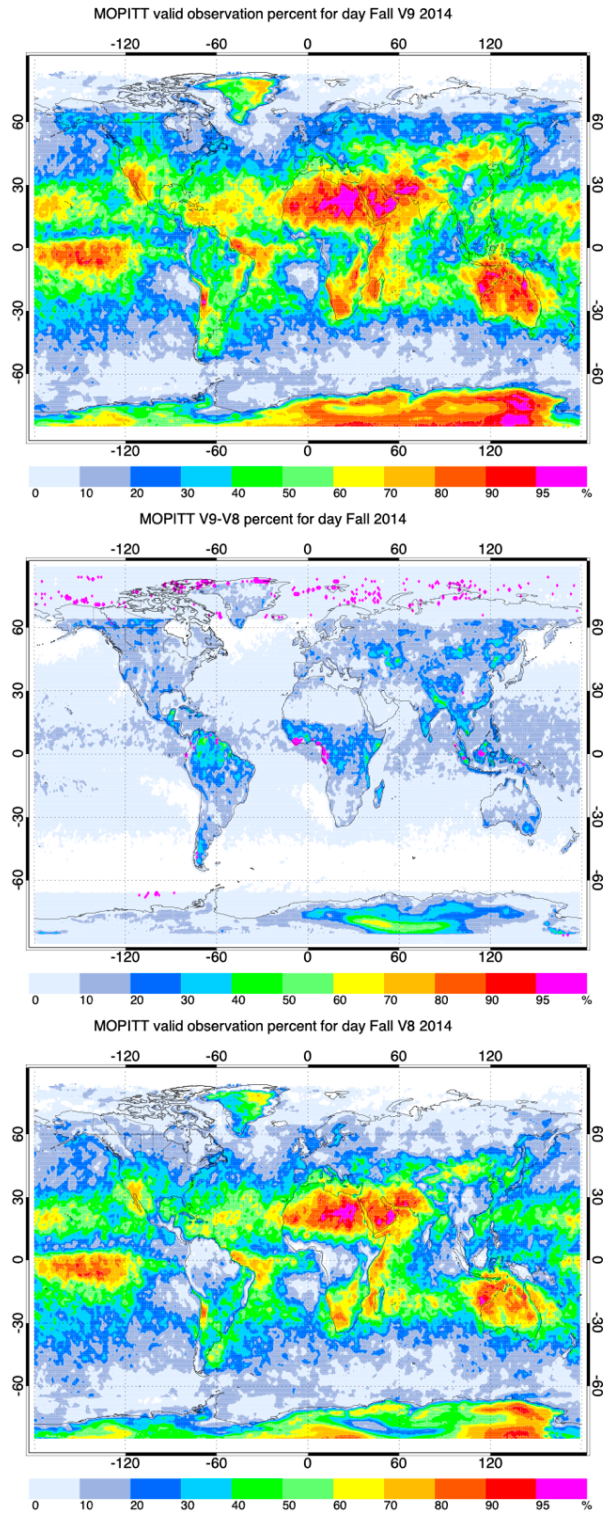
597

598 Figure (3) The same as Figure 2 but for spring season.





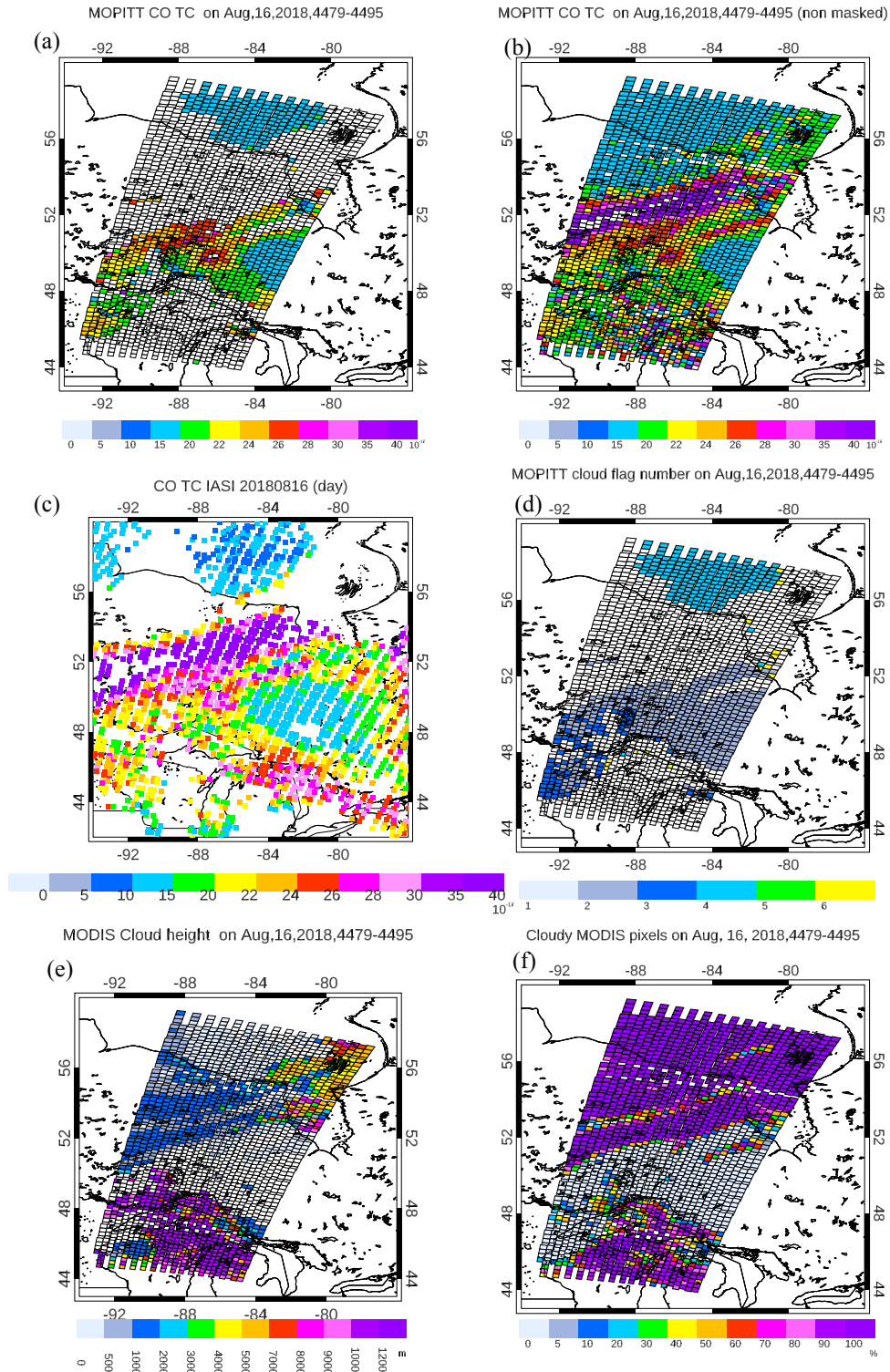
599  
 600 Figure (4) The same as Figure 2 but for summer season.  
 601



602

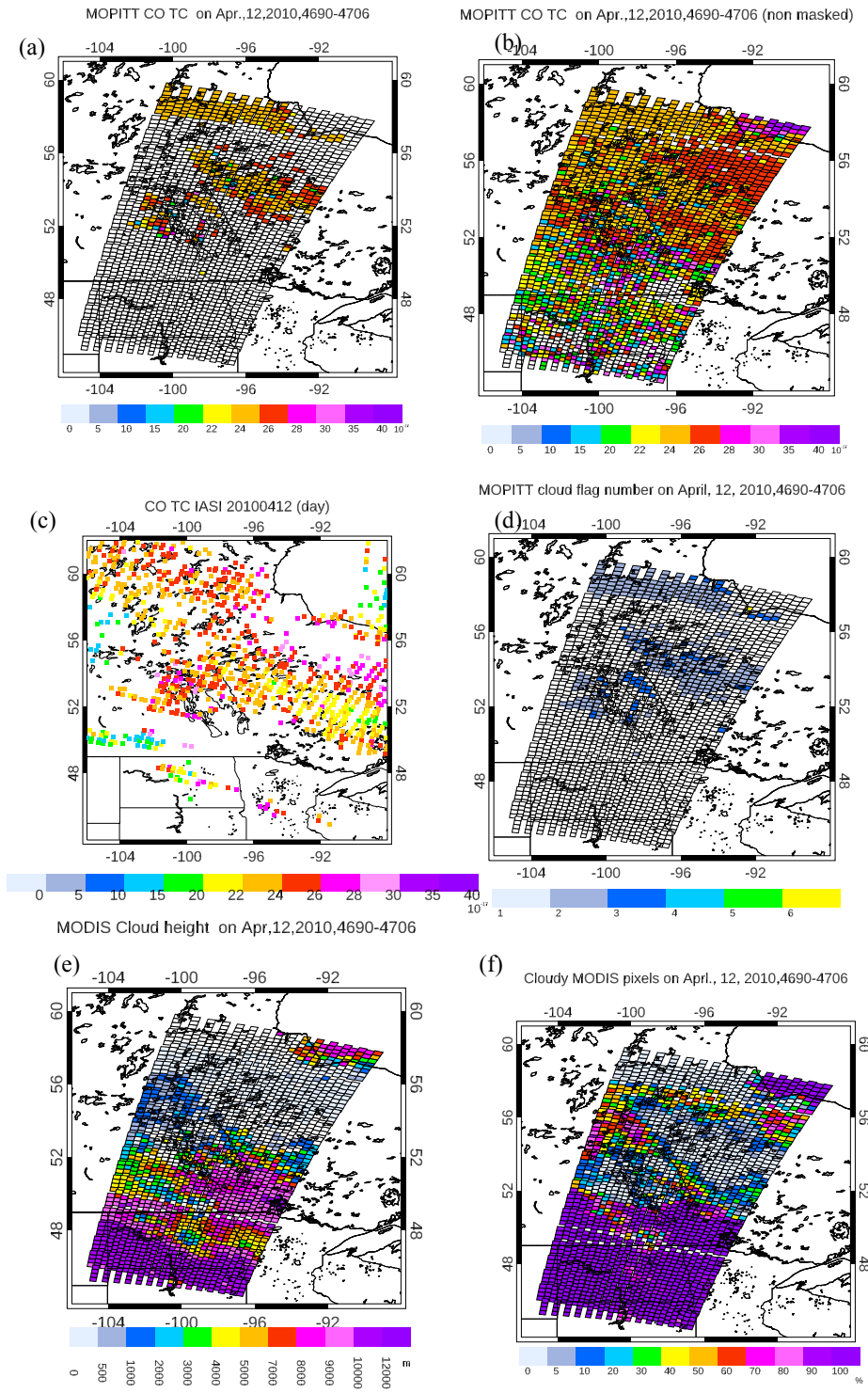
603 Figure (5) The same as Figure 2 but for fall season.

604



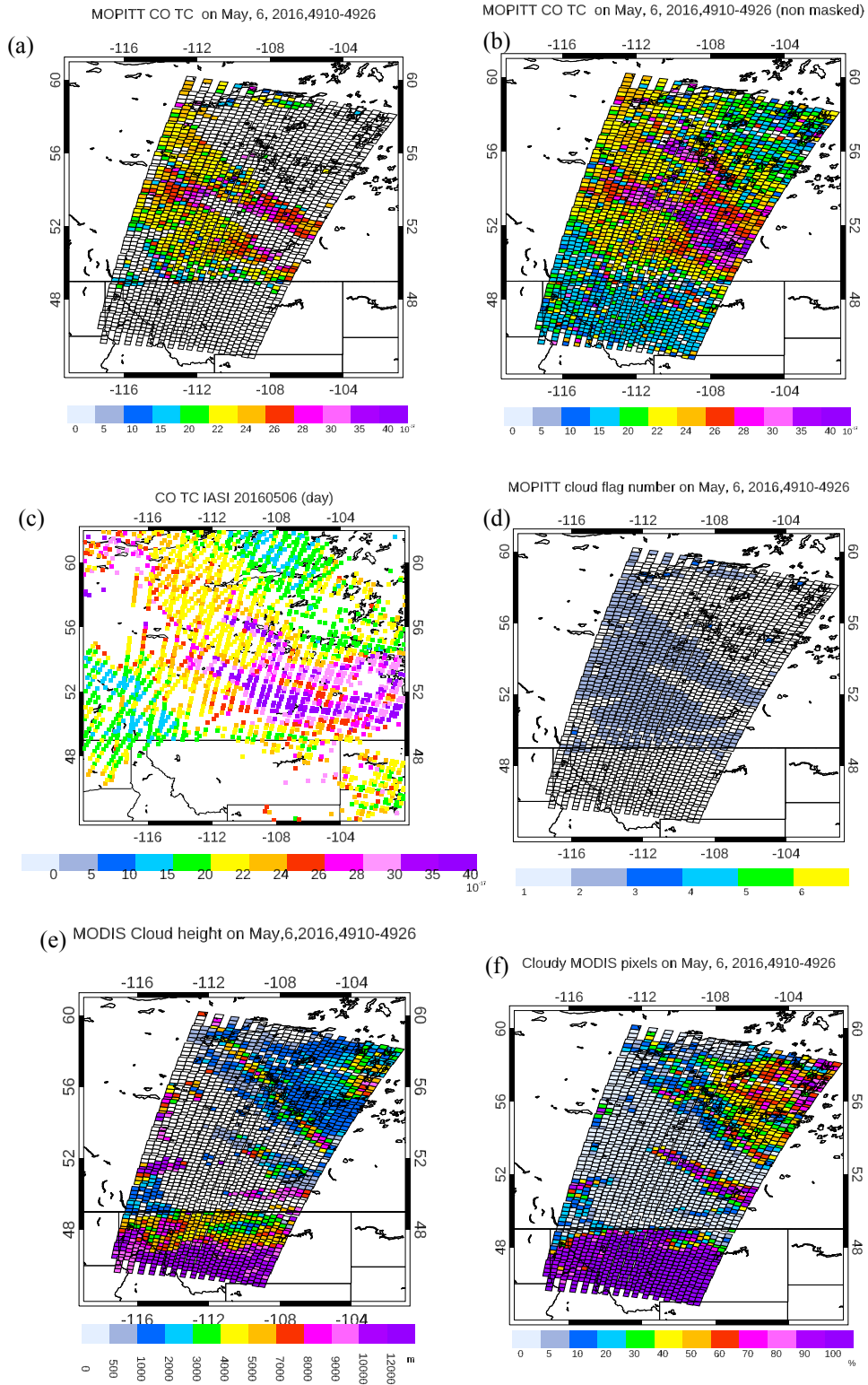
605  
 606 Figure 6. (a) Standard (cloud masked), (b) non-standard (non-cloud masked) CO TC, (c) IASI CO  
 607 TC, (d) MOPITT cloud flag number, (e) MODIS cloud height, and (f) cloud mask on 16 August,  
 608 2018. The faint black squares represent MOPITT pixels (22 km x 22 km) for all L1 observations.





610  
611  
612

Figure (7) The same as Figure 3, but for 12 April 2010.

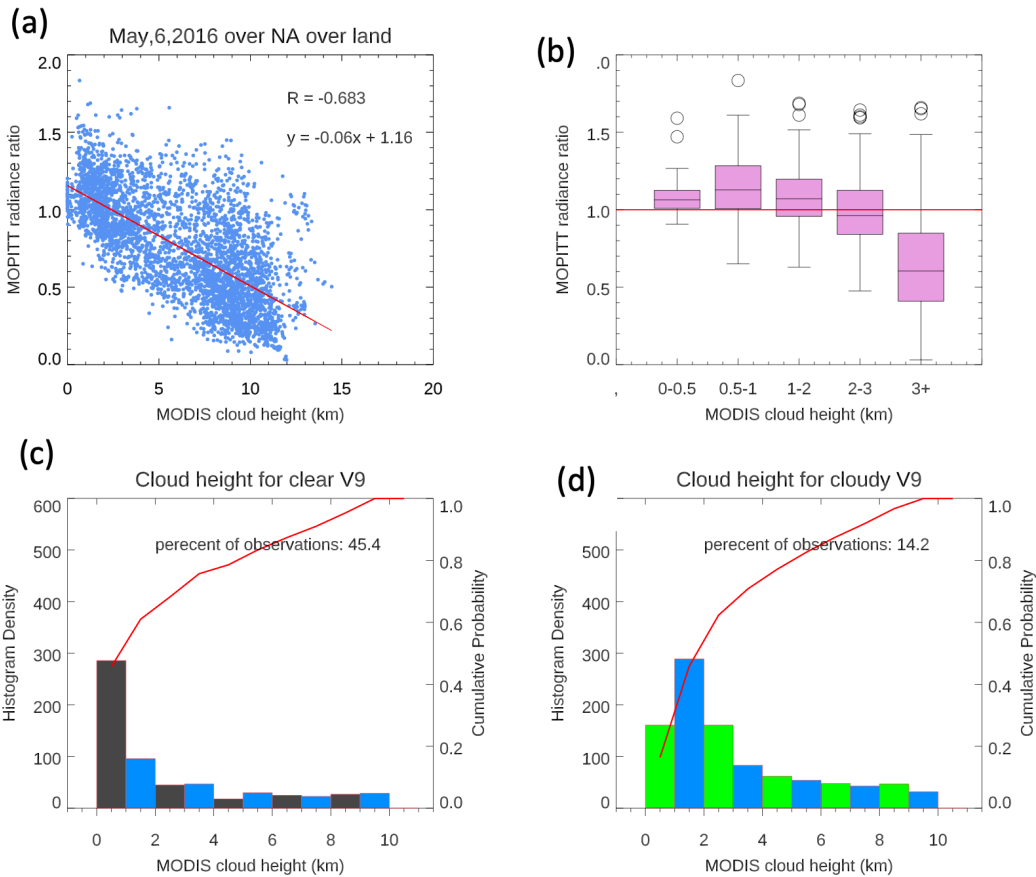


613  
614

615  
616

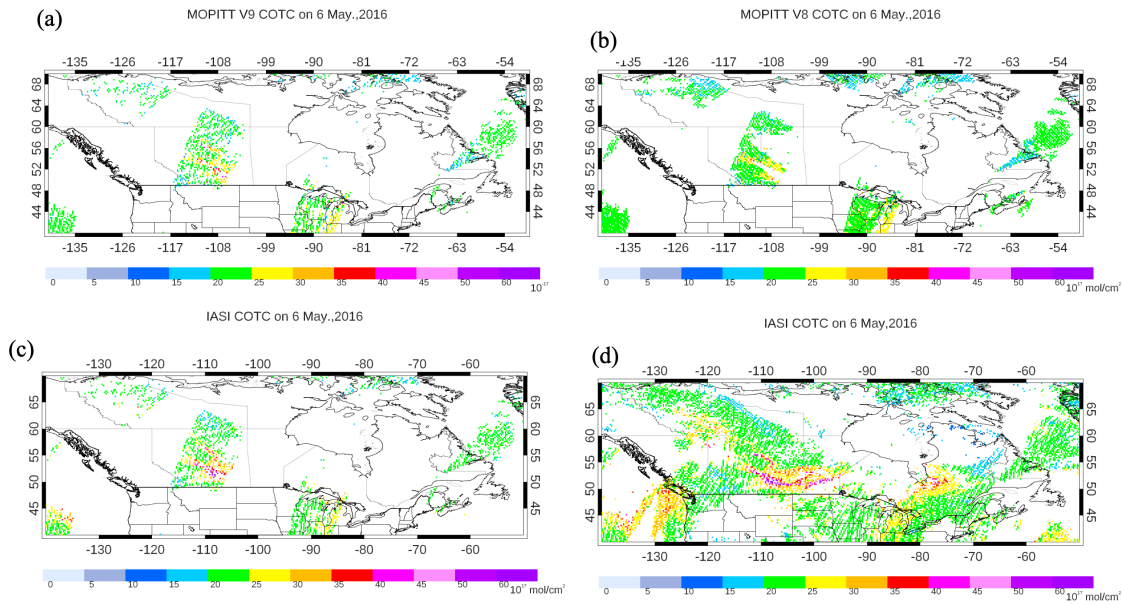
Figure (8) The same as Figure 3, but for 6 May 2016.

617



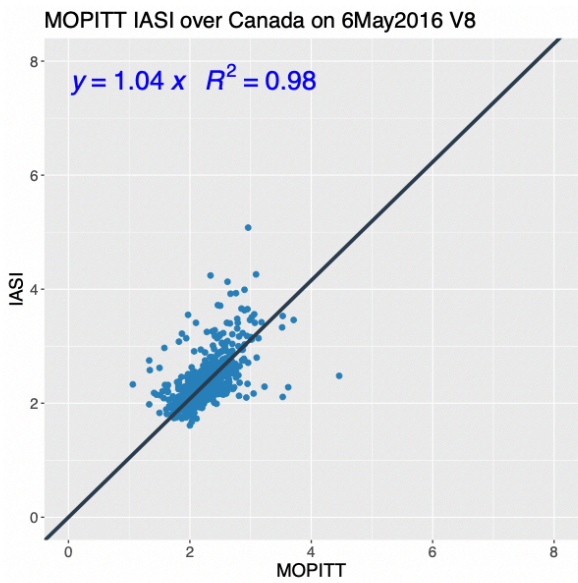
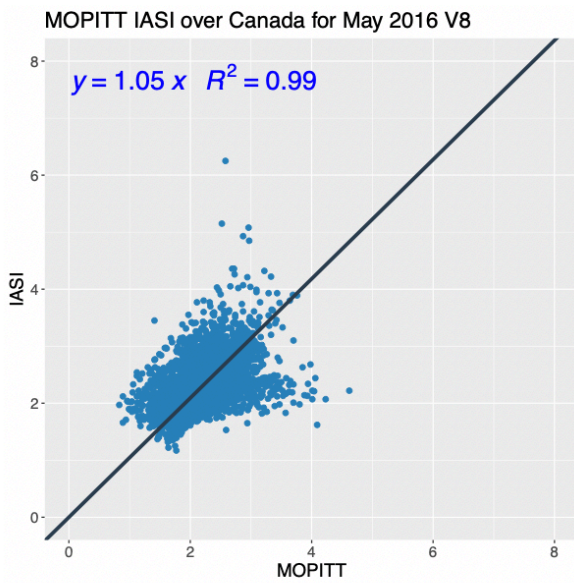
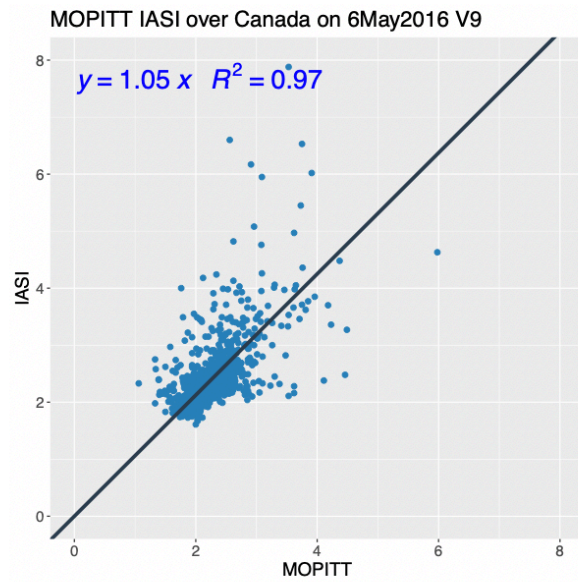
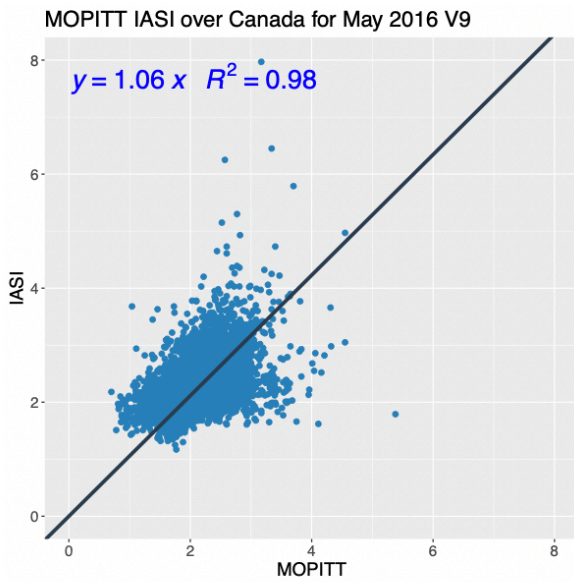
618

619 Figure (9) (a) scatter plot correlation between MOPITT radiance ratio (MRT) and MODIS cloud  
620 height, (b) A *Box and Whisker plot* of MRT and various MODIS cloud height groups, (c) The  
621 histogram density of MODIS cloud heights of MOPITT clear/MODIS clear observations, (d) The  
622 histogram density of MODIS cloud heights of MOPITT clear/MODIS cloudy observations on 6  
623 May 2016.



624  
 625 Figure (10) MOPITT CO total column for V9 (a) and V8 (b). IASI CO total column observations  
 626 of the corresponding with MOPITT (c) and the entire IASI CO retrievals (d) on 6 May 2016.  
 627

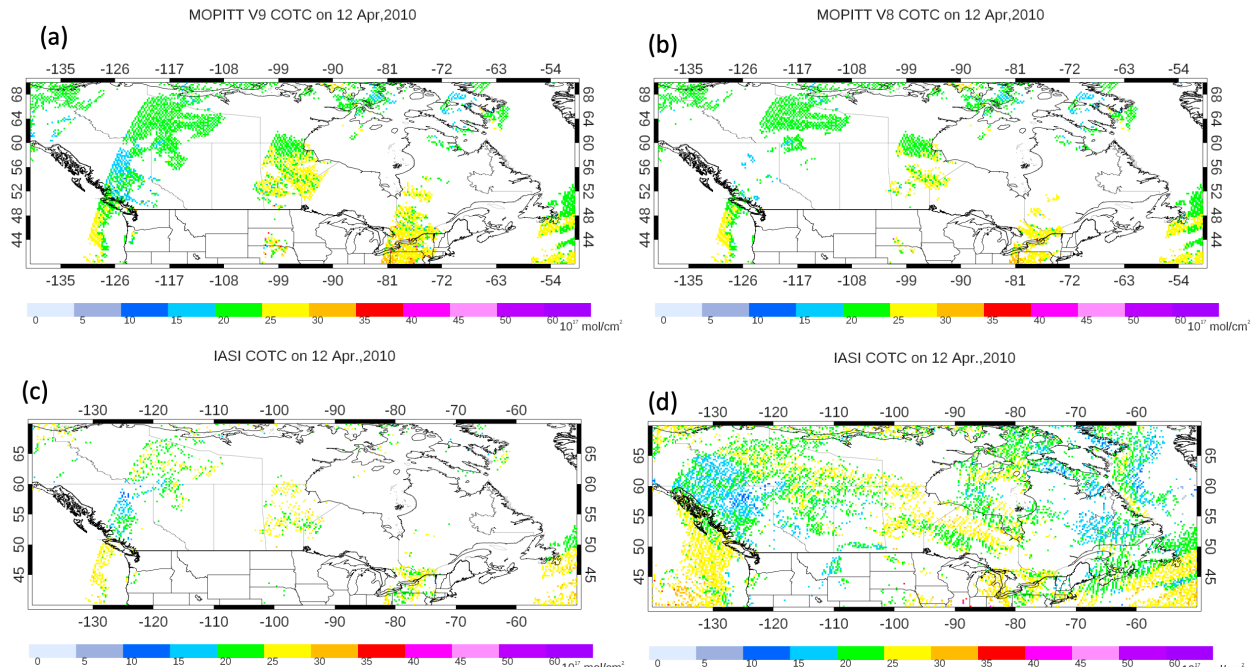




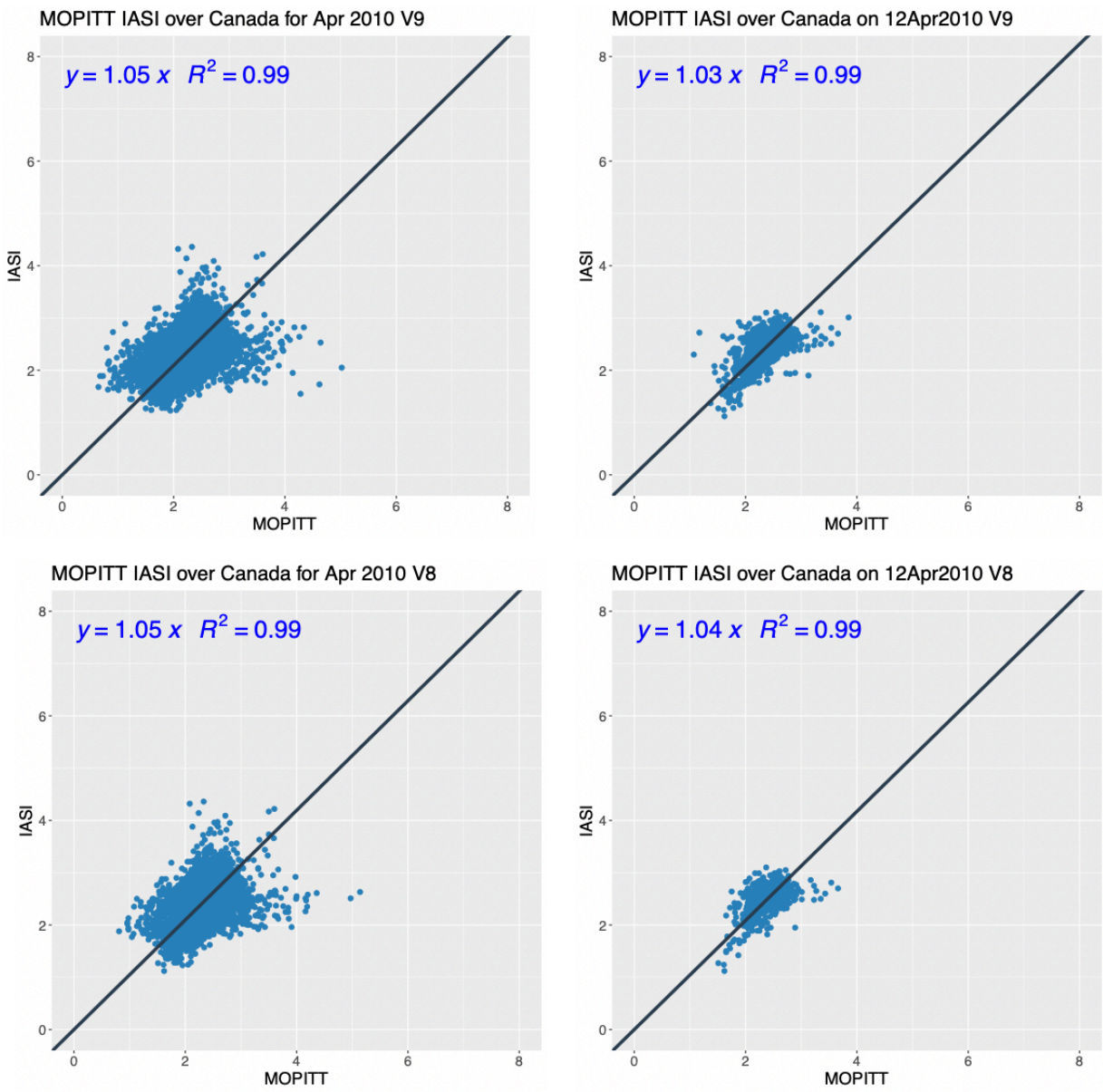
628

629 Figure (11) Scatter plots of the IASI and MOPITT CO retrievals in  $10^{18}$  molecules/cm<sup>2</sup>, for 6 May  
 630 2016 and the monthly averaged May 2016. The correlation coefficient and the regression slope are  
 631 reported.

632



633  
 634 Figure (12) The same as Figure 7, but for 12 April 2010.  
 635

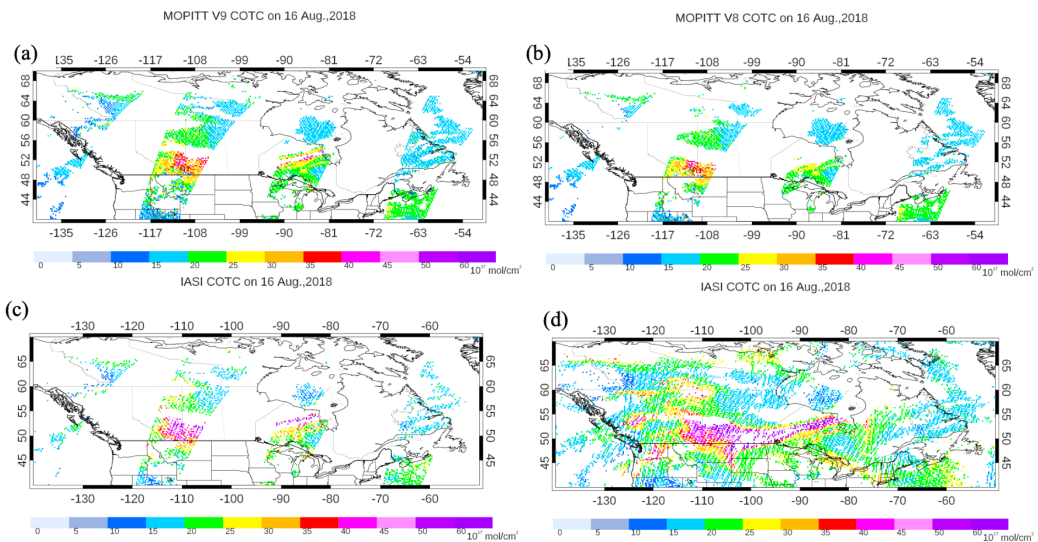


636

637

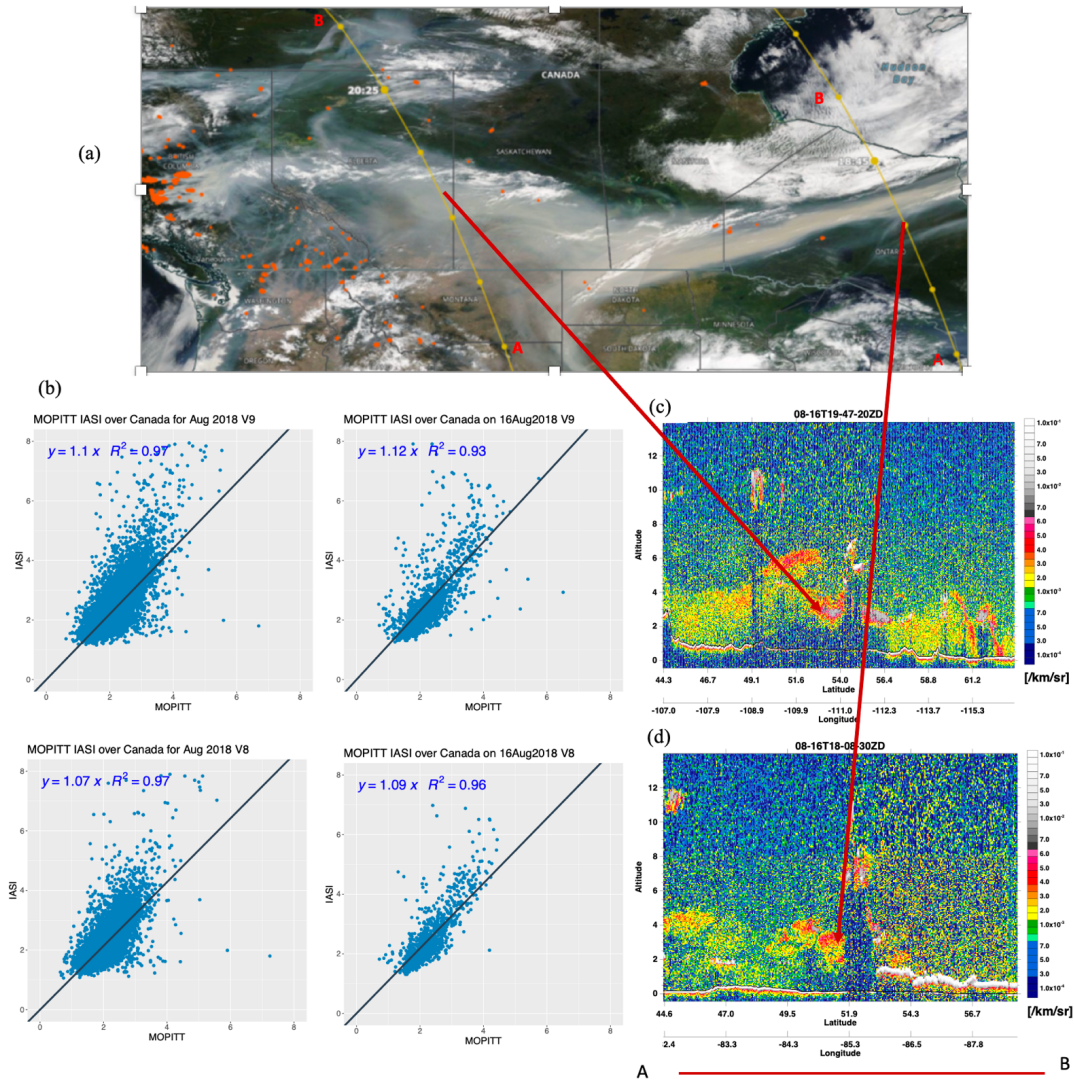
638 Figure (13) The same as Figure 8, but for 12 April 2010.

639



640  
 641 Figure (14) The same as Figure 3, but for 16 August 2018.





642  
 643 Figure (15) (a) MODIS Terra overlaid with fire points (red points), (b) scatter plots between IASI  
 644 and MOPITT TIR V9 and V8 and (c-d) daytime CALIPSO 532nm total attenuated backscatter on  
 645 16 August 2018.

646  
 647  
 648  
 649  
 650  
 651